Available online at www.sciencedirect.com
SCIENCE DIRECT®
Journal of Magnetic Resonance 174 (2005) 97–109
JMR Journal of Magnetic Resonance
www.elsevier.com/locate/jmr

Suppression of strong coupling artefacts in *J*-spectra ☆

Michael J. Thrippleton [b,*], Richard A.E. Edden [a], James Keeler [a]

[a] *Department of Chemistry, University of Cambridge, Lensfield Road, Cambridge CB2 1EW, UK*
[b] *Francis Bitter Magnet Laboratory, MIT, 170 Albany Street, Cambridge, MA 02139, USA*

Received 8 December 2004

Abstract

A major problem in *J*-resolved spectroscopy and many other experiments is the appearance of ''artefacts'' due to strong coupling. The signals giving rise to these artefacts follow the same coherence transfer pathways as the required signals, making it impossible to suppress them using phase cycling or pulsed field gradients. We present new methods for suppressing these artefacts, applicable to any experiment containing a *J*-resolved pulse sequence element, as well as to constant-time experiments.

Keywords: *J*-resolved spectroscopy; Strong coupling; Signal selection; Spatial variation; Constant time

1. Introduction

Two-dimensional *J*-spectroscopy offers the possibility of a complete separation of the effects of chemical shifts and (homonuclear) scalar couplings. This is achieved by first tilting the spectrum by 45° in frequency space; then, the projection in one direction gives a spectrum containing just a single line at each chemical shift, and a perpendicular cross-section taken at the position of each of these lines contains just the associated multiplet.

This separation of shifts and couplings is an attractive proposition as it enables the shifts to be identified in a straightforward way, and also allows each multiplet to be studied in isolation. For small- to medium-sized molecules, the *J*-spectrum may well allow the clear visualization of multiplets which are overlapping in the conventional spectrum.

Unfortunately, two drawbacks somewhat reduce the applicability of *J*-spectroscopy. First, as the signals are phase-modulated in both dimensions, the lines in the spectrum have the phase-twist lineshape, the 45° projection of which is identically zero. The original solution to this problem was to compute the absolute value of the spectrum before projection; however, this gives rise to very poor lineshapes in the projection. In turn, this problem has been addressed by using rather strong weighting functions, such as the ''pseudo-echo'' [1], to achieve a more acceptable lineshape. However, such weighting functions result in a loss of sensitivity and intensity distortions. Recently, it has been shown that the application of data processing not based on the Fourier transform can offer a solution to this lineshape problem, albeit at the expense of considerable complexity [2,3].

The second problem which besets *J*-spectra is that the presence of strong coupling leads to additional peaks in the spectrum which result in the appearance of lines in the projection which are *not* at the chemical shift. The presence of these extra lines detracts greatly from the attractive simplicity of the projection and makes its interpretation open to ambiguity. Peaks which arise

☆ This work was supported by the EPSRC, Procter & Gamble, and the Newton Trust; R.A.E.E. thanks Eli Lilly and Company Ltd for a CASE award. We are grateful to Dr. David Neuhaus for a generous allocation of spectrometer time at the MRC LMB.
* Corresponding author. Fax: +1 617 253 5405.
E-mail addresses: mjt32@mit.edu (M.J. Thrippleton), raee2@cam.ac.uk (R.A.E. Edden), James.Keeler@ch.cam.ac.uk (J. Keeler).

1090-7807/$ - see front matter © 2005 Elsevier Inc. All rights reserved.
doi:10.1016/j.jmr.2005.01.012

due to strong coupling are usually known as "strong coupling artefacts"; the term is something of a misnomer as the peaks are genuine and not the result of some imperfection in the experiment. However, the term is well established so we will continue to use it.

It should be noted that the same problem besets constant-time NMR experiments, as well as other experiments that contain a *J*-resolved or constant-time pulse sequence element [4–9].

As has been understood for many years [10–12], strong coupling artefacts arise from a mixing effect caused when a 180° pulse is applied to a strongly coupled spin system. The artefacts cannot be suppressed by phase cycling or pulsed field gradients, as the artefact signals originate from the same coherence transfer pathway as the required signals. In this paper we describe what we believe to be the first successful methods for suppressing these unwanted signals and show a number of different practical implementations to both *J*-spectroscopy and constant-time experiments [13].

2. *J*-spectroscopy

The pulse sequence for *J*-spectroscopy, shown in Fig. 1A, is simply a spin-echo of overall duration t_1 followed by data acquisition. As there is no mixing period, the resulting two-dimensional spectrum contains the same number of peaks as the conventional one-dimensional spectrum. However, since the spin-echo refocusses chemical shift (offset), but not the scalar coupling interaction, the frequency of each peak in the ω_1 (indirect) dimension is the same as that in the ω_2 (direct) dimension, but with chemical shift terms removed. Thus, a peak at Ω_I–πJ in the ω_2 dimension, where Ω_I is the offset of the spin and J is the coupling constant, has the frequency $-\pi J$ in the ω_1 dimension.

The *J*-spectrum of a two-spin system, 2,3-dibromothiophene, is shown in Fig. 2A. The four peaks clustered around $\omega_1 = 0$ are those expected for a weakly coupled spin system; when the spectrum is tilted by 45° these peaks line up into two pairs, as shown in Fig. 2B. Projection of this tilted spectrum (i.e., by adding up the data in the columns of the tilted spectrum) gives Fig. 2C; this projection contains a single peak at each of the two chemical shifts, with no splittings due to *J*-coupling.

In the spectrum of Fig. 2A, the peaks inside the dashed boxes are strong coupling artefacts. In the tilted spectrum these four peaks line up and so give rise to a single peak in the projection; it turns out that the peak is at the midpoint between the two chemical shifts. The suppression of this unwanted peak is the topic of this paper.

To understand the origin of the strong coupling artefacts, we first describe the operation of the pulse sequence in the weakly coupled case and then go on to introduce the effect of strong coupling. To make the connection between the two cases clear, we use the same operator method for both.

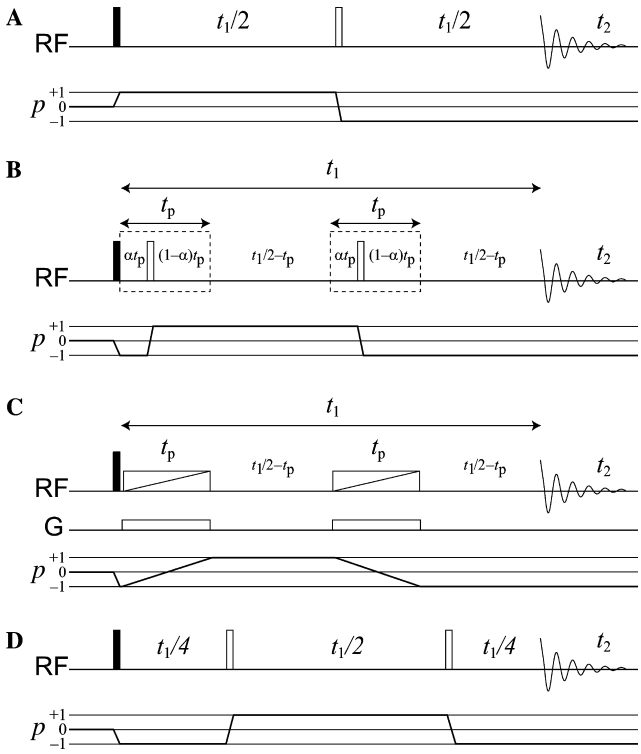

Fig. 1. Pulse sequences for two-dimensional *J*-spectroscopy, along with the required coherence transfer pathways: (A) the conventional single spin-echo pulse sequence; (B) sequence for multiple-scan suppression of strong coupling artefacts ($0 < \alpha < 1$); (C) sequence for single-scan suppression of strong coupling artefacts; (D) double spin-echo sequence. On the line marked RF, solid rectangles represent 90° pulses and open rectangles represent 180° pulses; rectangles with diagonal lines represent adiabatic swept-frequency pulses. Gradients required in sequence (C) are indicated on the lines marked G; gradients used for CTP selection in the other sequences are omitted in the figure.

3. *J*-spectroscopy—The weak coupling case

In this section, we compute the form of the *J*-spectrum for two weakly coupled spins in the weak coupling approximation, i.e.,

$$\hat{\mathcal{H}}_{FP} = \Omega_I \hat{I}_z + \Omega_S \hat{S}_z + 2\pi J \hat{I}_z \hat{S}_z,$$

where $\hat{\mathcal{H}}_{FP}$ is the free precession Hamiltonian.

Although there is nothing new in this calculation, it serves to introduce the operator method, which will then be carried forward to the strong coupling case.

3.1. Single-element basis operators

For a weakly coupled two-spin system the product functions ($|\alpha\alpha\rangle|\alpha\beta\rangle|\beta\alpha\rangle|\beta\beta\rangle$) are a good choice of basis as they are eigenfunctions of the free precession Hamiltonian $\hat{\mathcal{H}}_{FP}$. This means that during a period of free evo-

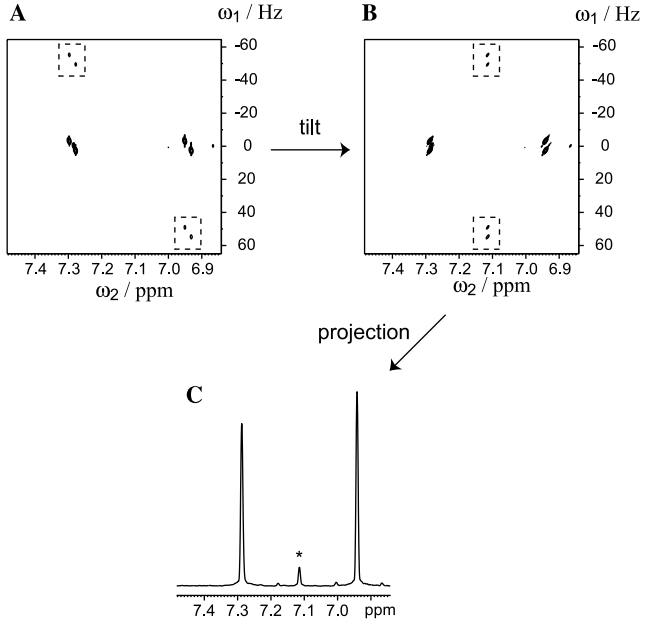

Fig. 2. (A) Experimental *J*-spectrum of 2,3-dibromothiophene in $CDCl_3$; the unwanted peaks due to strong coupling are enclosed by dashed boxes. Tilting the spectrum by 45° results in spectrum (B), in which chemical shift and coupling information are separated into the two dimensions. The projection of the tilted spectrum, obtained by summing the rows of (B), is shown in (C); this projection contains a singlet peak at each shift, without splitting due to coupling. The strong coupling artefacts give rise to the peak marked * in the projection. *Experimental*: the spectrum was recorded at 300 MHz; 8 scans per increment were recorded; CTP selection was achieved using equivalent gradient pulses (25%, 1 ms, half-sine shape) before and after the 180° pulse; the spectral widths in the ω_1 and ω_2 dimensions are 130 and 193 Hz, respectively; the acquisition time in t_2 was 2.7 s; 128 t_1 increments were recorded giving a maximum value of 1.0 s; the spectrum is processed using Gaussian pseudo-echo weighting functions in both dimensions and is displayed in magnitude mode.

lution the elements of the density matrix σ_{ij} evolve in a very simple way according to the following rule:

$$\sigma_{ij} \xrightarrow{\hat{\mathcal{H}}_{\mathrm{FP}}t} \sigma_{ij}\, \mathrm{e}^{\mathrm{i}(E_j - E_i)t}, \tag{1}$$

where E_i are the energies (in angular frequency units) of the basis functions, listed below:

number	basis function	energy
1	$\lvert\alpha\alpha\rangle$	$E_1 = \frac{1}{2}(\Omega_\mathrm{I} + \Omega_\mathrm{S} + \pi J)$,
2	$\lvert\alpha\beta\rangle$	$E_2 = \frac{1}{2}(\Omega_\mathrm{I} - \Omega_\mathrm{S} - \pi J)$,
3	$\lvert\beta\alpha\rangle$	$E_3 = \frac{1}{2}(-\Omega_\mathrm{I} + \Omega_\mathrm{S} - \pi J)$,
4	$\lvert\beta\beta\rangle$	$E_4 = \frac{1}{2}(-\Omega_\mathrm{I} - \Omega_\mathrm{S} + \pi J)$.

(2)

Thus, elements of the density matrix acquire a phase label during periods of free precession at a frequency determined by the energy levels of the system. In particular, the four elements representing coherences of order −1 give rise to the four lines in the one-dimensional spectrum.

It is useful to describe the density operator for the spin system in terms of *single-element basis operators*—operators that represent single elements of the density matrix. For example, $\hat{I}_-\hat{S}_\alpha$ represents σ_{31}, and therefore evolves at the frequency $E_1 - E_3 = \Omega_\mathrm{I} + \pi J$ during free precession:

$$\hat{I}_-\hat{S}_\alpha \xrightarrow{\hat{\mathcal{H}}_{\mathrm{FP}}t} \exp[\mathrm{i}(\Omega_\mathrm{I} + \pi J)t]\hat{I}_-\hat{S}_\alpha.$$

3.2. Analysis of the pulse sequence

We will now use these single-element operators to describe the spectrum which arises from the *J*-spectroscopy pulse sequence shown in Fig. 1A. The density operator at equilibrium can be written $\hat{I}_z + \hat{S}_z$, and the initial 90° pulse (for convenience taken to be about the *y*-axis) generates transverse magnetization according to

$$\hat{I}_z + \hat{S}_z \xrightarrow{\frac{\pi}{2}\hat{F}_y} \hat{I}_x + \hat{S}_x.$$

The resulting operators are then written in terms of the single-element basis operators to give

$$\hat{I}_x + \hat{S}_x = \tfrac{1}{2}(\hat{I}_+\hat{S}_\alpha + \hat{I}_+\hat{S}_\beta + \hat{I}_\alpha\hat{S}_+ + \hat{I}_\beta\hat{S}_+ + \hat{I}_-\hat{S}_\alpha + \hat{I}_-\hat{S}_\beta + \hat{I}_\alpha\hat{S}_- + \hat{I}_\beta\hat{S}_-).$$

The last four terms have coherence order −1 and, according to the CTP given in Fig. 1A, do not contribute to the observed signal and so can be ignored. The first four terms do give rise to observed signals. For example, the $\hat{I}_\beta\hat{S}_+$ term evolves at the frequency $-(\Omega_\mathrm{S} - \pi J)$ during the first period of free precession, acquiring a phase label:

$$\hat{I}_\beta\hat{S}_+ \xrightarrow{\frac{1}{2}t_1(\Omega_\mathrm{I}\hat{I}_z + \Omega_\mathrm{S}\hat{S}_z + 2\pi J\hat{I}_z\hat{S}_z)} \exp[-\tfrac{1}{2}\mathrm{i}(\Omega_\mathrm{S} - \pi J)t_1]\hat{I}_\beta\hat{S}_+.$$

The 180° pulse then changes the sign of the coherence order and converts $\hat{I}_\beta$ to $\hat{I}_\alpha$:

$$\exp[-\tfrac{1}{2}\mathrm{i}(\Omega_\mathrm{S} - \pi J)t_1]\hat{I}_\beta\hat{S}_+ \xrightarrow{\pi\hat{F}_x} \exp[-\tfrac{1}{2}\mathrm{i}(\Omega_\mathrm{S} - \pi J)t_1]\hat{I}_\alpha\hat{S}_-.$$

This operator now evolves during the second half of the spin-echo:

$$\exp[-\tfrac{1}{2}\mathrm{i}(\Omega_\mathrm{S} - \pi J)t_1]\hat{I}_\alpha\hat{S}_- \xrightarrow{\frac{1}{2}t_1(\Omega_\mathrm{I}\hat{I}_z + \Omega_\mathrm{S}\hat{S}_z + 2\pi J\hat{I}_z\hat{S})t_1} \exp[+\tfrac{1}{2}\mathrm{i}(\Omega_\mathrm{S} + \pi J)t_1]\exp[-\tfrac{1}{2}\mathrm{i}(\Omega_\mathrm{S} - \pi J)t_1]\hat{I}_\alpha\hat{S}_-,$$

which simplifies to

$$\exp[+\mathrm{i}\pi J t_1]\hat{I}_\alpha\hat{S}_-.$$

During the acquisition time t_2 the operator evolves at the frequency $\Omega_\mathrm{S} + \pi J$ to give

$$\exp[+\mathrm{i}\pi J t_1]\exp[+\mathrm{i}(\Omega_\mathrm{S} + \pi J)t_2]\hat{I}_\alpha\hat{S}_-.$$

The overall result is that in the two-dimensional spectrum this term gives rise to a single peak at $(\Omega_\mathrm{S} + \pi J)$

in the direct (ω_2) dimension, and at $+\pi J$ in the indirect (ω_1) dimension; note that the signal is phase-modulated in t_1 and so the corresponding peak will have the phase-twist lineshape. The same analysis can be applied to all four operators to obtain the full spectrum. The result is that peaks appear at their usual positions in the ω_2 dimension, while their frequencies in the ω_1 dimension are equal to the frequencies in ω_2 with the offset terms removed.

4. *J*-spectroscopy—The strong coupling case

We now use a similar operator method to compute the form of the *J*-spectrum in the strongly coupled case, i.e.,

$$\hat{\mathcal{H}}_{\mathrm{FP}} = \Omega_{\mathrm{I}}\hat{I}_z + \Omega_{\mathrm{S}}\hat{S}_z + 2\pi J\hat{\mathbf{I}}\cdot\hat{\mathbf{S}}.$$

4.1. Single-element basis operators

In a strongly coupled system, the product basis functions are no longer the eigenfunctions of $\hat{\mathcal{H}}_{\mathrm{FP}}$, so the above analysis is no longer valid. Fortunately, the convenience of this approach can be regained by choosing a new set of basis functions that *are* the eigenfunctions of $\hat{\mathcal{H}}_{\mathrm{FP}}$. These can be found using standard methods [14] and are listed here, together with the corresponding eigenvalues (in rad s^{-1}):

number	basis function	energy
1	$\lvert\alpha\alpha\rangle$	$E_1 = \frac{1}{2}(\Omega_{\mathrm{I}} + \Omega_{\mathrm{S}} + \pi J)$,
2	$\cos\theta\lvert\alpha\beta\rangle - \sin\theta\lvert\beta\alpha\rangle$	$E_2 = \frac{1}{2}(\Delta\Omega - \pi J)$,
3	$\cos\theta\lvert\beta\alpha\rangle + \sin\theta\lvert\alpha\beta\rangle$	$E_3 = \frac{1}{2}(-\Delta\Omega - \pi J)$,
4	$\lvert\beta\beta\rangle$	$E_4 = \frac{1}{2}(-\Omega_{\mathrm{I}} - \Omega_{\mathrm{S}} + \pi J)$.

The *strong coupling parameter* θ, which indicates the strength of the coupling interaction, is defined as

$$\tan 2\theta = \frac{2\pi J}{\Omega_{\mathrm{S}} - \Omega_{\mathrm{I}}},$$

and the *positive* quantity $\Delta\Omega$ is defined as

$$\Delta\Omega = \sqrt{(\Omega_{\mathrm{I}} - \Omega_{\mathrm{S}})^2 + 4\pi^2 J^2}.$$

$\Delta\Omega$ is approximately equal to the chemical shift difference. The definition of θ assumes that $\Omega_{\mathrm{S}} > \Omega_{\mathrm{I}}$ and $J > 0$. It can be seen that as $\theta \to 0$, the basis functions and their energies collapse to their weak coupling counterparts described in Section 3.1.

In this basis, the evolution of the density matrix elements during free precession obeys Eq. (1) once again. We can define a new set of single-element basis operators that represent the 16 elements of σ in the new basis:

$$\begin{array}{cccc} & \{\hat{I}_+\hat{S}_+\} & & \\ \{\hat{I}_+\hat{S}_\alpha\} & \{\hat{I}_+\hat{S}_\beta\} & \{\hat{I}_\alpha\hat{S}_+\} & \{\hat{I}_\beta\hat{S}_+\} \\ & \{\hat{I}_+\hat{S}_-\} & \{\hat{I}_-\hat{S}_+\} & \\ \{\hat{I}_-\hat{S}_\alpha\} & \{\hat{I}_-\hat{S}_\beta\} & \{\hat{I}_\alpha\hat{S}_-\} & \{\hat{I}_\beta\hat{S}_-\} \\ & \{\hat{I}_-\hat{S}_-\}. & & \end{array}$$

This notation makes explicit the connection of the operators to their weak coupling counterparts, while acknowledging the difference by the use of curly braces. For example, $\{\hat{I}_-\hat{S}_\alpha\}$ represents σ_{31} when $\hat{\sigma}$ is written in the strong coupling basis, just as $\hat{I}_-\hat{S}_\alpha$ represents σ_{31} when $\hat{\sigma}$ is written in the product basis. In the limit $\theta \to 0$, the two bases are identical and $\{\hat{I}_-\hat{S}_\alpha\} \to \hat{I}_-\hat{S}_\alpha$.

The evolution of these operators during free precession is straightforward to describe, but the effect of a RF pulse is considerably more complex than in the weakly coupled case.

4.2. Free precession

During free precession, the single-element operators are phase-modulated at frequencies which depend on the energy levels. For example, in the weak coupling case the operator $\hat{I}_-\hat{S}_\alpha$ represents the matrix element σ_{31} and so evolves at a frequency $E_1 - E_3$:

$$\text{weak coupling}: \quad \hat{I}_-\hat{S}_\alpha \xrightarrow{\hat{\mathcal{H}}_{\mathrm{FP}}t} \exp[\mathrm{i}(E_1 - E_3)t]\hat{I}_-\hat{S}_\alpha.$$

We saw that in the weak coupling case, $E_1 - E_3 = \Omega_{\mathrm{I}} + \pi J$ so the evolution can be written

$$\text{weak coupling}: \quad \hat{I}_-\hat{S}_\alpha \xrightarrow{\hat{\mathcal{H}}_{\mathrm{FP}}t} \exp[\mathrm{i}(\Omega_{\mathrm{I}} + \pi J)t]\hat{I}_-\hat{S}_\alpha.$$

In the strongly coupled case the element σ_{31} is represented by the operator $\{\hat{I}_-\hat{S}_\alpha\}$; again this evolves at frequency $E_1 - E_3$, where the energies are now those appropriate for strong coupling:

$$\text{strong coupling}: \quad \{\hat{I}_-\hat{S}_\alpha\} \xrightarrow{\hat{\mathcal{H}}_{\mathrm{FP}}t} \exp[\mathrm{i}(E_1 - E_3)t]\{\hat{I}_-\hat{S}_\alpha\}.$$

This frequency $E_1 - E_3$ we write as $\{\Omega_{\mathrm{I}} + \pi J\}$; the idea of this notation is that it gives an approximate idea of the frequency, while acknowledging that the actual frequency is modified as a result of strong coupling. In the limit $\theta \to 0$, the curly braces disappear and $\{\Omega_{\mathrm{I}} + \pi J\} \to \Omega_{\mathrm{I}} + \pi J$. Using this approach, the evolution is written

$$\{\hat{I}_-\hat{S}_\alpha\} \xrightarrow{\hat{\mathcal{H}}_{\mathrm{FP}}t} \exp[\mathrm{i}\{\Omega_{\mathrm{I}} + \pi J\}t]\{\hat{I}_-\hat{S}_\alpha\}.$$

The precise value of $\{\Omega_{\mathrm{I}} + \pi J\}$ can be calculated explicitly from the energy levels of the system:

$$\{\Omega_{\mathrm{I}} + \pi J\} \equiv E_1 - E_3 = \tfrac{1}{2}\Omega_{\mathrm{I}} + \tfrac{1}{2}\Omega_{\mathrm{S}} - \tfrac{1}{2}\Delta\Omega + \pi J.$$

4.3. Pulses

While the evolution of coherences during free precession is similar in the weakly and strongly coupled cases, the effects of RF pulses on coherences are very different. Consider, for example, the effect of a 180° pulse on the coherence $\hat{I}_\beta\hat{S}_+$ in a weakly coupled system

$$\hat{I}_\beta\hat{S}_+ \overset{\pi\hat{F}_x}{\rightarrow} \hat{I}_\alpha\hat{S}_-$$

the pulse simply changes the sign of the coherence order and, loosely speaking, changes the state of spin I. Crucially, the operators represent transverse magnetization on spin S before and after the pulse: a 180° pulse does not transfer coherence from one spin to the other.

The effect of the pulse on the coherence $\{\hat{I}_\beta\hat{S}_+\}$ in a strongly coupled system is rather different

$$\{\hat{I}_\beta\hat{S}_+\} \overset{\pi\hat{F}_x}{\rightarrow} \cos 2\theta\{\hat{I}_\alpha\hat{S}_-\} + \sin 2\theta\{\hat{I}_-\hat{S}_\alpha\},$$

where θ is the strong coupling parameter, defined above. The term proportional to $\cos 2\theta$ represents magnetization transferred in the same way as in the weak coupling case: +1-quantum coherence on spin S is converted to −1-quantum coherence on the same spin. However, a part of the magnetization, proportional to $\sin 2\theta$, is transferred to −1-quantum coherence on spin I; in other words, a 180° pulse causes coherence transfer in a strongly coupled spin system.[1]

4.4. Analysis of the pulse sequence

The coherence transfer caused by the 180° pulse is the origin of the strong coupling artefacts seen in J-spectra. Consider a part of the magnetization that is transferred from one spin to the other by the 180° pulse: during the first part of the spin-echo the magnetization evolves at the offset of spin I, whereas after the 180° pulse it evolves at the offset of spin S. So, rather than the offset being refocussed, as it usually is in a spin-echo, we end up with magnetization which appears to have evolved at half the difference between the offsets of the two spins. This conclusion can be demonstrated by the following calculation.

In Section 3.2, we determined, for a weakly coupled system, the fate of the $\hat{I}_\beta\hat{S}_+$ operator present at the start of t_1; it was shown that this term gives rise to a peak at $(\omega_1,\omega_2) = (\pi J, \Omega_S + \pi J)$. We now perform the same analysis for the operator $\{\hat{I}_\beta\hat{S}_+\}$ in a strongly coupled spin system.

This operator first acquires a phase label during the initial $t_1/2$ delay:

$$\{\hat{I}_\beta\hat{S}_+\} \overset{\frac{1}{2}\hat{\mathcal{H}}_{FP}t_1}{\longrightarrow} \exp[-\tfrac{1}{2}\mathrm{i}\{\Omega_S - \pi J\}t_1]\{\hat{I}_\beta\hat{S}_+\}.$$

The 180° pulse then causes partial coherence transfer, as described above:

$$\exp[-\tfrac{1}{2}\mathrm{i}\{\Omega_S - \pi J\}t_1]\{\hat{I}_\beta\hat{S}_+\} \overset{\pi\hat{F}_x}{\rightarrow} \cos 2\theta \exp[-\tfrac{1}{2}\mathrm{i}\{\Omega_S - \pi J\}t_1]\{\hat{I}_\alpha\hat{S}_-\} + \sin 2\theta \exp[-\tfrac{1}{2}\mathrm{i}\{\Omega_S - \pi J\}t_1]\{\hat{I}_-\hat{S}_\alpha\}.$$

These two operators then acquire a further phase label during the second $t_1/2$ delay:

$$\begin{aligned}&\cos 2\theta \exp[-\tfrac{1}{2}\mathrm{i}\{\Omega_S - \pi J\}t_1]\{\hat{I}_\alpha\hat{S}_-\} + \sin 2\theta \\ &\quad\times \exp[-\tfrac{1}{2}\mathrm{i}\{\Omega_S - \pi J\}t_1]\{\hat{I}_-\hat{S}_\alpha\} \overset{\frac{1}{2}\hat{\mathcal{H}}_{FP}t_1}{\longrightarrow} \cos 2\theta \\ &\quad\times \exp[\tfrac{1}{2}\mathrm{i}(\{\Omega_S + \pi J\} - \{\Omega_S - \pi J\})t_1]\{\hat{I}_\alpha\hat{S}_-\} + \sin 2\theta \\ &\quad\times \exp[\tfrac{1}{2}\mathrm{i}(\{\Omega_I + \pi J\} - \{\Omega_S - \pi J\})t_1]\{\hat{I}_-\hat{S}_\alpha\}.\end{aligned}$$

Substituting the explicit frequencies in place of the quantities in curly braces, this expression simplifies to

$$\begin{aligned}&\cos 2\theta \exp[+\mathrm{i}\pi J t_1]\{\hat{I}_\alpha\hat{S}_-\} \\ &\quad + \sin 2\theta \exp[\mathrm{i}(\pi J - \tfrac{1}{2}\Delta\Omega)t_1]\{\hat{I}_-\hat{S}_\alpha\},\end{aligned} \tag{3}$$

where, as before, $\Delta\Omega$ is given by

$$\Delta\Omega = \sqrt{(\Omega_I - \Omega_S)^2 + 4\pi^2 J^2}.$$

The first term in Eq. (3) gives rise to a peak at $(\omega_1,\omega_2) = (\pi J, \{\Omega_S + \pi J\})$; this corresponds to the peak observed in the weakly coupled spectrum. The second term gives rise to a peak at $(\pi J - \frac{1}{2}\Delta\Omega, \{\Omega_I + \pi J\})$; this peak, which is not present in the weakly coupled spectrum, results from coherence that is transferred by the 180° pulse. For small θ, this peak will be the weaker of the two.

A full density matrix calculation can be used to determine the position and intensity of every peak in the spectrum. This type of calculation can be performed symbolically using a program such as *Mathematica*, but the resulting expressions tend to be unwieldy, especially for the more complicated pulse sequences we will describe later. The expressions were therefore expanded as Taylor series in θ, and all terms in θ^2 and higher powers were discarded; this results in relatively simple expressions that are valid for small θ, i.e., a modest degree of strong coupling.

For the two-spin system, there are eight peaks in the J-spectrum; the frequencies and intensities are listed in Table 1. There are four peaks of the type found in weakly coupled spectra and four only found in strongly coupled spectra (the "artefacts"); the latter are displaced from the normal peaks in ω_1 by $\frac{1}{2}\Delta\Omega$. When a magnitude calculation is performed and the 45° projection taken, the strong coupling artefacts appear at the mean of the two chemical shifts.

[1] Strictly speaking, in a strongly coupled spin system coherences can no longer be assigned to individual spins; however, for small θ we may say that $\{\hat{I}_\beta\hat{S}_+\}$ represents +1-quantum coherence that is *predominantly* associated with spin S.

Table 1
Frequencies and amplitudes of peaks in a strongly coupled J-spectrum; the amplitudes are given to first order in θ

ω_1 frequency	ω_2 frequency	Amplitude	
$+\pi J$	$\{\Omega_S + \pi J\}$	$\frac{1}{2}$	
$+\pi J - \frac{1}{2}\Delta\Omega$	$\{\Omega_S + \pi J\}$	$-\theta$	s
$-\pi J$	$\{\Omega_S - \pi J\}$	$\frac{1}{2}$	
$-\pi J - \frac{1}{2}\Delta\Omega$	$\{\Omega_S - \pi J\}$	$+\theta$	s
$+\pi J$	$\{\Omega_I + \pi J\}$	$\frac{1}{2}$	
$+\pi J + \frac{1}{2}\Delta\Omega$	$\{\Omega_I + \pi J\}$	$+\theta$	s
$-\pi J$	$\{\Omega_I - \pi J\}$	$\frac{1}{2}$	
$-\pi J + \frac{1}{2}\Delta\Omega$	$\{\Omega_I - \pi J\}$	$-\theta$	s

The peaks which are only present in a strongly coupled spectrum are marked with a "s".

5. Suppression of strong coupling artefacts

The strong coupling artefacts observed in J-spectra are caused by coherence transfer during the 180° pulse, i.e., by the "$\sin 2\theta$" terms. Since these terms have the same coherence order as the required "$\cos 2\theta$" terms, the artefacts are not eliminated by phase cycling or pulsed field gradients. In this section, we present three methods for suppressing the artefacts, while retaining the required peaks.

5.1. Multiple-scan suppression

Fig. 1B shows a pulse sequence which gives rise to a J-spectrum in which strong coupling artefacts are suppressed. Although this sequence contains *two* 180° pulses instead of one, it is equivalent to the conventional J-spectroscopy pulse sequence in the weak coupling approximation: offsets are refocussed, scalar coupling evolves throughout, and the resulting J-spectrum is the same. Furthermore, the value of the parameter α has no effect on the signal.

In a strongly coupled spin system, however, the sequence has a subtly different effect, since coherence transfer may occur during *neither*, *either* or *both* of the 180° pulses. As a result, three types of peak occur:

1. "Normal" peaks result from coherence that is transferred by *neither* of the 180° pulses. These are the peaks present in the weakly coupled case and are usually the most intense in the spectrum.
2. "First-order" strong coupling artefacts result from coherence transfer that is caused by *one* of the 180° pulses. For modest strong coupling, the intensity of these peaks will be proportional to θ.
   The peaks associated with coherence transfer during the *first* 180° pulse appear at the same position in the spectrum as the normal peaks, since the first pulse is not "moved" as t_1 is incremented. The first order peaks caused by coherence transfer during the *second* 180° pulse appear at the same frequency as the artefacts in the simple J-spectroscopy experiment, since this pulse is moved at the same rate as in the simple experiment.
3. "Second order" strong coupling artefacts result from magnetization that is transferred to the coupled spin by the first 180° pulse and then back again by the second. These peaks can be neglected when θ is small, since their intensities are second order in θ.

The phases of the first-order artefacts depend on α, while the phases of the normal peaks do not. Thus, by repeating the experiment with different values of α and co-adding the data, the artefacts can be suppressed. The sequence therefore acts as a filter, allowing the normal peaks to appear in the spectrum, while attenuating the artefacts.

To understand how this works, it is helpful to consider why the phase of the signals in a weakly coupled system does not depend on α. This is because the offset evolution during the first αt_p period is cancelled by that during the second αt_p period; likewise, the offset evolution during the first $(1-\alpha)t_p$ period is cancelled by that during the second $(1-\alpha)t_p$ period.

However, if coherence transfer occurs as a result of the first 180° pulse, the offset will be different during the two αt_p periods, and so the offset evolution will not cancel. Likewise, if coherence transfer occurs as a result of the second 180° pulse, the offset will be different during the two $(1-\alpha)t_p$ periods and again the offset evolution will not cancel. Thus, the first-order strong coupling artefacts acquire a phase that depends on α and on the difference between the two offsets.

This conclusion can be confirmed using the operator approach. By way of example, we consider the term $\{\hat{I}_\alpha \hat{S}_-\}$, present after the 90° pulse, and follow its evolution through the pulse sequence. For simplicity, we will consider that part of the signal which does not experience coherence transfer during the first 180° pulse, but does experience coherence transfer during the second 180° pulse. It will be shown that this pathway gives rise to a strong coupling peak, and that this peak has a phase which depends on α.

The period of free precession before the 180° pulse gives rise to a phase label:

$$\{\hat{I}_\alpha \hat{S}_-\} \xrightarrow{\hat{\mathcal{H}}_{FP}(\alpha t_p)} \exp[i\{\Omega_S + \pi J\}\alpha t_p]\{\hat{I}_\alpha \hat{S}_-\}.$$

A 180° pulse is then applied; as noted above, only the term that is *not* the result of coherence transfer, i.e., the "$\cos 2\theta$" term, is included on the right-hand side:

$$\exp[i\{\Omega_S + \pi J\}\alpha t_p]\{\hat{I}_\alpha \hat{S}_-\} \xrightarrow{\pi \hat{F}_x} \cos 2\theta \exp[i\{\Omega_S + \pi J\}\alpha t_p] \times \{\hat{I}_\beta \hat{S}_+\}.$$

Free precession then continues for a period $t_1/2$:

$$\cos 2\theta \exp[\mathrm{i}\{\Omega_S + \pi J\}\alpha t_p]\{\hat{I}_\beta \hat{S}_+\} \xrightarrow{\frac{1}{2}\hat{\mathcal{H}}_{FP} t_1} \cos 2\theta \times \exp[\mathrm{i}\{\Omega_S + \pi J\}\alpha t_p] \exp[-\tfrac{1}{2}\mathrm{i}\{\Omega_S - \pi J\}t_1]\{\hat{I}_\beta \hat{S}_+\}.$$

The second 180° pulse is then applied; this time, only the term that *is* the result of coherence transfer, i.e., the "$\sin 2\theta$" term, is included on the right-hand side:

$$\cos 2\theta \exp[\mathrm{i}\{\Omega_S + \pi J\}\alpha t_p] \exp[-\tfrac{1}{2}\mathrm{i}\{\Omega_S - \pi J\}t_1]\{\hat{I}_\beta \hat{S}_+\} \xrightarrow{\pi \hat{F}_x} \times \sin 2\theta \cos 2\theta \exp[\mathrm{i}\{\Omega_S + \pi J\}\alpha t_p] \times \exp[-\tfrac{1}{2}\mathrm{i}\{\Omega_S - \pi J\}t_1]\{\hat{I}_- \hat{S}_\alpha\}.$$

Finally, free precession occurs for a period $(1-\alpha)t_p + (t_1/2 - t_p) = t_1/2 - \alpha t_p$:

$$\sin 2\theta \cos 2\theta \exp[\mathrm{i}\{\Omega_S + \pi J\}\alpha t_p] \exp[-\tfrac{1}{2}\mathrm{i}\{\Omega_S - \pi J\}t_1] \times \{\hat{I}_- \hat{S}_\alpha\} \xrightarrow{\hat{\mathcal{H}}_{FP}(\frac{1}{2}t_1 - \alpha t_p)} \sin 2\theta \cos 2\theta \exp[\mathrm{i}\{\Omega_I + \pi J\} \times (\tfrac{1}{2}t_1 - \alpha t_p)] \exp[\mathrm{i}\{\Omega_S + \pi J\}\alpha t_p] \exp[-\tfrac{1}{2}\mathrm{i}\{\Omega_S - \pi J\}t_1]\{\hat{I}_- \hat{S}_\alpha\}.$$

Substituting for the frequency terms in curly braces, the final expression simplifies to

$$\sin 2\theta \cos 2\theta \exp[\mathrm{i}\alpha \Delta\Omega t_p] \exp[\mathrm{i}(\pi J - \tfrac{1}{2}\Delta\Omega)t_1]\{\hat{I}_- \hat{S}_\alpha\}.$$

This term gives rise to a strong coupling artefact at $(\pi J - \frac{1}{2}\Delta\Omega, \{\Omega_I + \pi J\})$, which is at the same frequency as was predicted for the basic *J*-spectroscopy pulse sequence in Section 4.4. The crucial difference is that the signal now has an α-dependent phase factor $\exp[\mathrm{i}\alpha\Delta\Omega t_p]$. The signal can therefore be averaged to zero by the co-addition of several experiments with different values of α.

In the simplest form of the experiment, α is varied from 0 to 1 in N equal steps, and the signal attenuation factor is given by the following summation:

$$A = \frac{1}{N}\left|\sum_{n=1}^{N} \exp\left[+\mathrm{i}\frac{n-1}{N-1}\Delta\Omega t_p\right]\right|.$$

A is plotted as a function of $\Delta\Omega$ in Fig. 3 for a typical set of experimental parameters. The degree of attenuation deteriorates at low values of $\Delta\Omega$, and A is periodic; this behaviour is analogous to that of a traditional *z*-filter for the suppression of zero-quantum coherence as a function of the zero-quantum frequency [15]. However, for the present application the periodicity is less worrysome, since the size of strong coupling artefacts decreases with increasing chemical shift difference. A plot of A as a function of t_p gives a similar graph.

The frequencies and complex amplitudes of all the peaks in the two-dimensional spectrum were obtained via density matrix calculations and are listed in Table 2. All of the strong coupling signals have the form derived above and are attenuated by the same factor.

Fig. 4 compares projections of *J*-spectra of 2,3-dibromothiophene recorded using the conventional sequence, Fig. 4A, and using the multiple-scan filter described here, Fig. 4B. It is evident that a high degree of suppression of the strong coupling artefacts is obtained by the latter sequence.

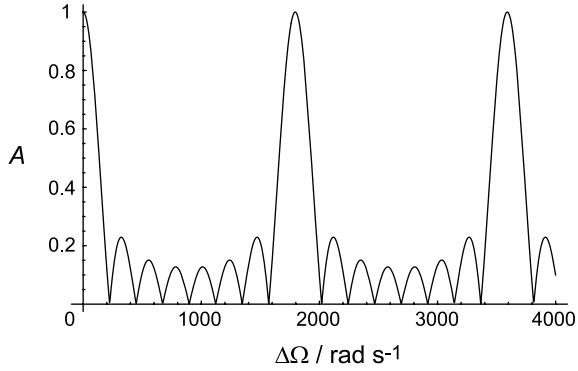

Fig. 3. Predicted attenuation factor versus $\Delta\Omega$ for the multiple-scan filter. The calculation assumes that spectra are acquired with 8 evenly spaced values of α, between 0 and 1, with $t_p = 24.5$ ms.

Table 2
Frequencies and amplitudes of peaks in a strongly coupled *J*-spectrum, obtained with the pulse sequence of Fig. 1B; the amplitudes are given to first order in the strong coupling parameter θ and the peaks which are only present in a strongly coupled spectrum are marked with a "s"

ω_1 frequency	ω_2 frequency	Complex amplitude	
$+\pi J$	$\{\Omega_S + \pi J\}$	$\frac{1}{2} - \theta$	
$+\pi J$	$\{\Omega_S + \pi J\}$	$+\theta\exp[-\mathrm{i}\alpha\Delta\Omega t_p]$	s
$+\pi J + \frac{1}{2}\Delta\Omega$	$\{\Omega_S + \pi J\}$	$-\theta\exp[-\mathrm{i}\alpha\Delta\Omega t_p]$	s
$-\pi J$	$\{\Omega_S - \pi J\}$	$\frac{1}{2} + \theta$	
$-\pi J$	$\{\Omega_S - \pi J\}$	$-\theta\exp[-\mathrm{i}\alpha\Delta\Omega t_p]$	s
$-\pi J + \frac{1}{2}\Delta\Omega$	$\{\Omega_S - \pi J\}$	$+\theta\exp[-\mathrm{i}\alpha\Delta\Omega t_p]$	s
$+\pi J$	$\{\Omega_I + \pi J\}$	$\frac{1}{2} + \theta$	
$+\pi J$	$\{\Omega_I + \pi J\}$	$-\theta\exp[+\mathrm{i}\alpha\Delta\Omega t_p]$	s
$+\pi J - \frac{1}{2}\Delta\Omega$	$\{\Omega_I + \pi J\}$	$+\theta\exp[+\mathrm{i}\alpha\Delta\Omega t_p]$	s
$-\pi J$	$\{\Omega_I - \pi J\}$	$\frac{1}{2} - \theta$	
$-\pi J$	$\{\Omega_I - \pi J\}$	$+\theta\exp[+\mathrm{i}\alpha\Delta\Omega t_p]$	s
$-\pi J - \frac{1}{2}\Delta\Omega$	$\{\Omega_I - \pi J\}$	$-\theta\exp[+\mathrm{i}\alpha\Delta\Omega t_p]$	s

The main disadvantage of this approach is that suppression is only achieved by co-adding experiments with different values of α. When several scans are needed to achieve the required sensitivity, the filter will not increase the total experiment time. In other cases, suppression will be achieved at a considerable time cost. 2D *J*-resolved spectroscopy nevertheless remains a relatively short experiment, due to the small spectral width required in the indirect dimension.

A second disadvantage is that the minimum t_1 value is $2t_p$ rather than zero, so relaxation reduces the intensity of the signal by a factor of $\exp(-2t_p/T_2)$. For small molecules, this sensitivity loss should not be too great. Another consequence of the inability to generate data at $t_1 = 0$ is a frequency-dependent phase factor. However, as the data are generally processed to give a magnitude spectrum, this phase factor is not of any significance.

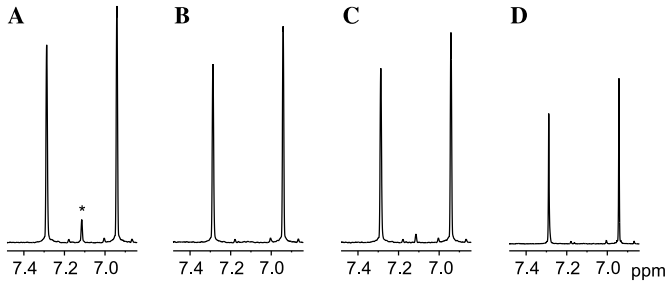

Fig. 4. Projections of the tilted *J*-spectra of 2,3-dibromothiophene, obtained with (A) the conventional pulse sequence, (B) a multiple-scan filter, (C) a single-scan filter, and (D) the DSE *J*-spectroscopy experiment with symmetrization of the tilted spectrum; the strong coupling artefact is marked with a star. *Experimental*: suppression of strong coupling artefacts was achieved in (B) by a filter with eight evenly spaced values of α and duration $t_p = 24.5$ ms, and in (C) using adiabatic 180° CHIRP pulses. For these pulses the frequency was swept through 4.5 kHz in $t_p = 24.5$ ms; the radiofrequency field strength was constant at 400 Hz during the sweeps, except during the first and final tenths, when it was smoothed to zero using the first and second quarter periods of a sine function. During the CHIRP a magnetic field gradient of strength 0.9% of the maximum ($\approx$60 G cm^{-1}) was applied. The experiments were recorded with 8 scans per t_1 increment; CTP selection in (B) was achieved using pairs of equivalent gradient pulses before and after the 180° pulses (27 and 17% strength, 1 ms duration, half-sine shape); other relevant parameters are as given in the caption to Fig. 2.

The following two sections describe alternative suppression methods which avoid one or both of these disadvantages.

5.2. Single-scan suppression

To achieve suppression of strong coupling artefacts in a single scan, we employed the technique of spatial variation, which has been successfully used to accelerate other NMR experiments [16–18]. Fig. 1C shows the resulting *J*-spectroscopy pulse sequence. As described in our earlier work [19–22], the combination of a swept-frequency 180° pulse with a gradient acts as a 180° pulse, the timing of which depends on position in the sample. The pulse sequence is therefore the same as a multiple-scan sequence in which the value of α varies with position. The resulting signal is equivalent to that obtained using a multiple-scan filter with an infinite number of different α values.

It should be noted that in contrast to the zero-quantum suppression technique we described previously [21,22], the required magnetization is dephased by the first sweep-gradient element. Fortunately, in the pulse sequence proposed here the magnetization is rephased during the second sweep; however, there will be some loss of signal due to diffusion and convection.

The projection from a *J*-spectrum of 2,3-dibromothiophene recorded using the single-scan filter is shown in

Table 3
Frequencies and amplitudes of peaks in the DSE *J*-spectrum; the amplitudes are given to first order in θ, and the peaks which are only present in a strongly coupled spectrum are marked with a "s"

ω_1 frequency	ω_2 frequency	Amplitude	
$+\pi J$	$\{\Omega_S + \pi J\}$	$\frac{1}{2} - \theta$	
$+\pi J - \frac{1}{4}\Delta\Omega$	$\{\Omega_S + \pi J\}$	θ	s
$+\pi J + \frac{1}{4}\Delta\Omega$	$\{\Omega_S + \pi J\}$	$-\theta$	s
$-\pi J$	$\{\Omega_S - \pi J\}$	$\frac{1}{2} + \theta$	
$-\pi J - \frac{1}{4}\Delta\Omega$	$\{\Omega_S - \pi J\}$	$-\theta$	s
$-\pi J + \frac{1}{4}\Delta\Omega$	$\{\Omega_S - \pi J\}$	θ	s
$+\pi J$	$\{\Omega_I + \pi J\}$	$\frac{1}{2} + \theta$	
$+\pi J - \frac{1}{4}\Delta\Omega$	$\{\Omega_I + \pi J\}$	$-\theta$	s
$+\pi J + \frac{1}{4}\Delta\Omega$	$\{\Omega_I + \pi J\}$	$-\theta$	s
$-\pi J$	$\{\Omega_I - \pi J\}$	$\frac{1}{2} - \theta$	
$-\pi J - \frac{1}{4}\Delta\Omega$	$\{\Omega_I - \pi J\}$	$-\theta$	s
$-\pi J + \frac{1}{4}\Delta\Omega$	$\{\Omega_I - \pi J\}$	θ	s

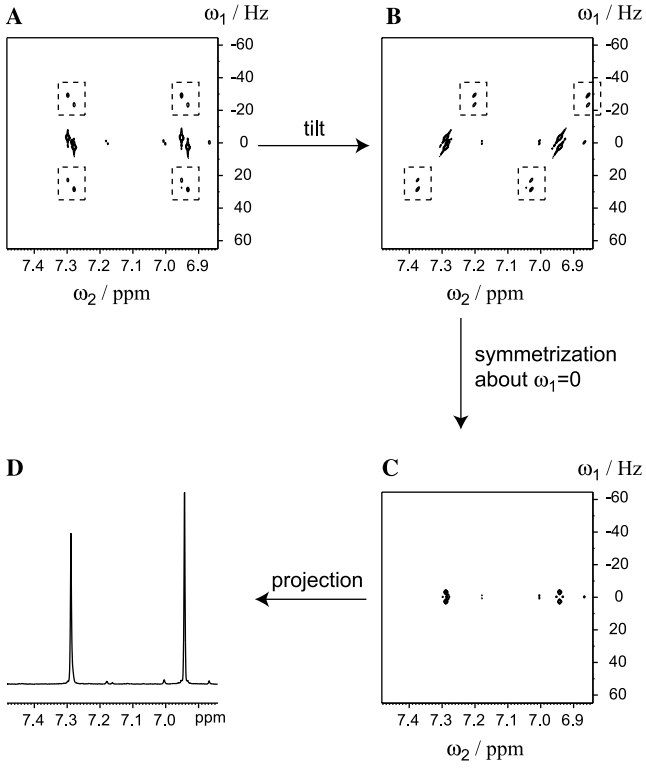

Fig. 5. (A) DSE *J*-spectrum of 2,3-dibromothiophene. (B) When the spectrum is tilted, the strong coupling artefacts are no longer related to one another by reflection through $\omega_1 = 0$. (C) Symmetrization therefore removes the artefacts and a clean projection (D) results. *Experimental*: relevant parameters are as given in the caption to Fig. 2.

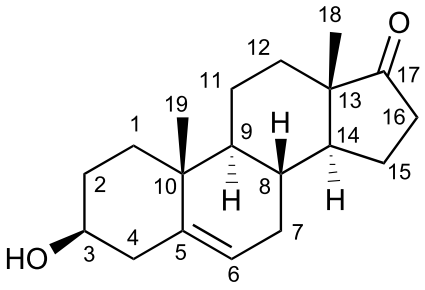

Fig. 6. Structure of dehydroisoandrosterone (5-androsten-3β-ol-17-one). An NMR sample was prepared by dissolving 44 mg in $CDCl_3$ (1 ml).

Fig. 4C. There is significant suppression of the strong coupling artefact, but the suppression is not as good as that obtained using the multiple-scan filter. To date, we have been unable to identify the precise reason for this underperformance. It is possible, however, that the simple interpretation of the sweep-gradient element given above is undermined by the fact that "strength" of the coupling increases as the swept field approaches resonance with the spins—the effect utilized in TOCSY experiments. Further developments in this regard will be reported.

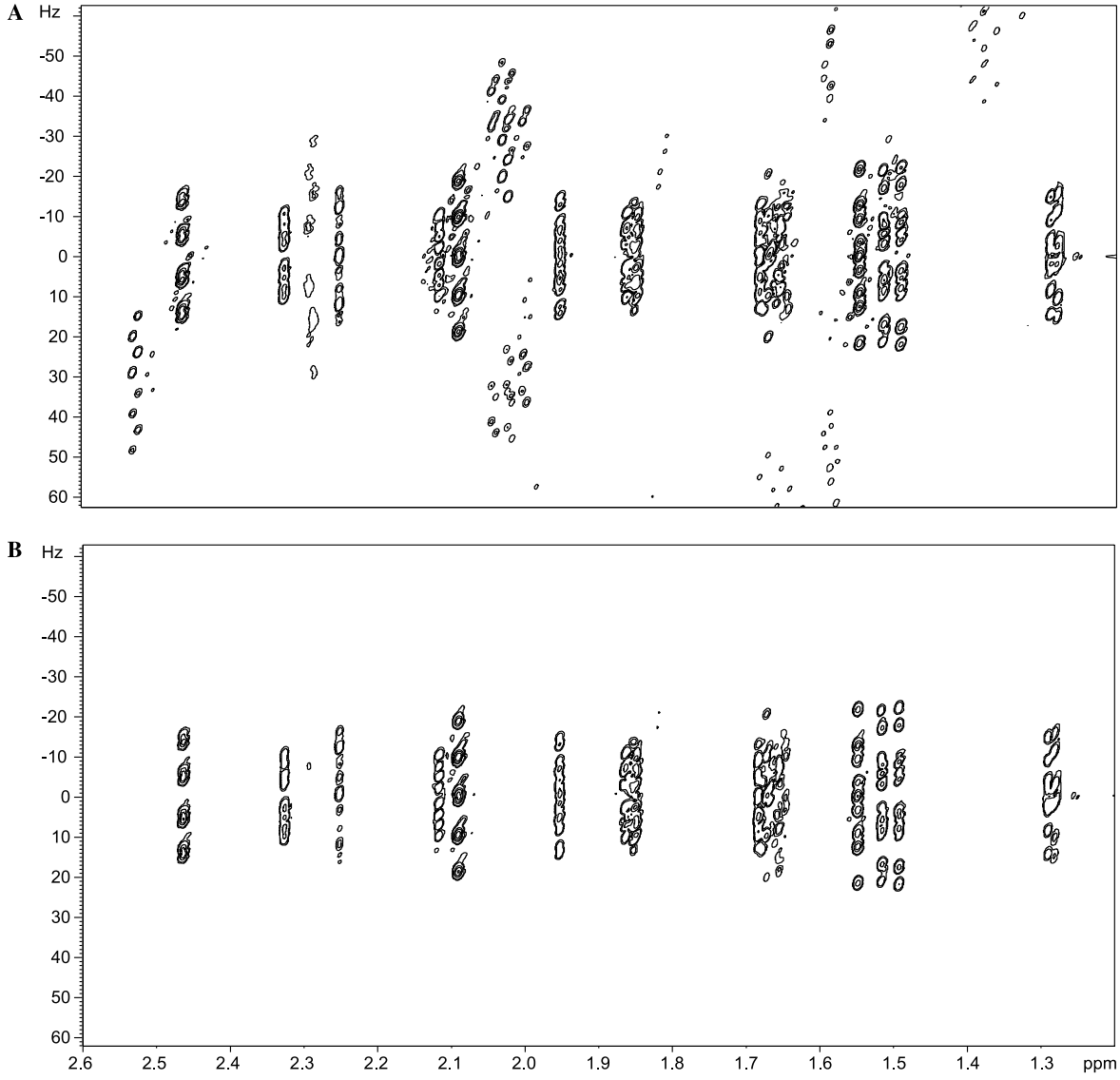

Fig. 7. Tilted *J*-spectra of dehydroisoandrosterone. Spectrum (A) was acquired with the conventional sequence and spectrum (B) with the multiple-scan filter. Note that the strong coupling artefacts in the bottom lefthand corner of the spectra do not appear to have symmetry-related partners in F_1. This is caused by the peak being folded in F_1 and the tilting procedure therefore not pairing up the artefacts. *Experimental*: suppression of strong coupling artefacts was achieved in (B) using a filter with 8 evenly spaced values of α and duration $t_p = 24$ ms. Both spectra were acquired at 500 MHz with 8 scans per t_1 increment; spectral widths in the ω_1 and ω_2 dimensions are 125 Hz and 3 kHz, respectively; the acquisition time in t_2 was 2.7 s; 256 t_1 increments were recorded giving a maximum value of 2.0 s; the spectrum has been processed using Gaussian pseudo-echo weighting functions in both dimensions and is displayed in magnitude mode. CTP selection was achieved with pairs of equivalent half-sine shaped 1 ms gradients either side of the 180° pulses (40% strength around the first 180° pulse in both experiments and 60% strength around the second in (B)).

5.3. Symmetry-based suppression

In this section, a third method, called double spin-echo (DSE) *J*-spectroscopy, is proposed for the suppression of strong coupling artefacts; this is also a single-scan method and further avoids the potential relaxation or diffusion losses associated with the multiple- or single-scan suppression methods described above. The pulse sequence, shown in Fig. 1D, consists of two spin-echoes of equal duration. No repetition is required and the strong coupling artefacts are not immediately suppressed. However, the symmetry properties of the artefacts in the ω_1 dimension are such that they can be removed by suitable data processing.

In the conventional *J*-spectroscopy experiment, the 180° pulse generates strong coupling artefacts that are displaced from the normal peaks by $\pm\frac{1}{2}\Delta\Omega$. As t_1 increases in the DSE *J*-spectroscopy experiment, each spin-echo expands at *half* the rate of the single echo in the conventional experiment: each refocussing pulse therefore generates artefacts displaced by half the amount observed in the original experiment, i.e., by $\pm\frac{1}{4}\Delta\Omega$. The frequencies and complex amplitudes of all of the peaks were calculated and are listed in Table 3.

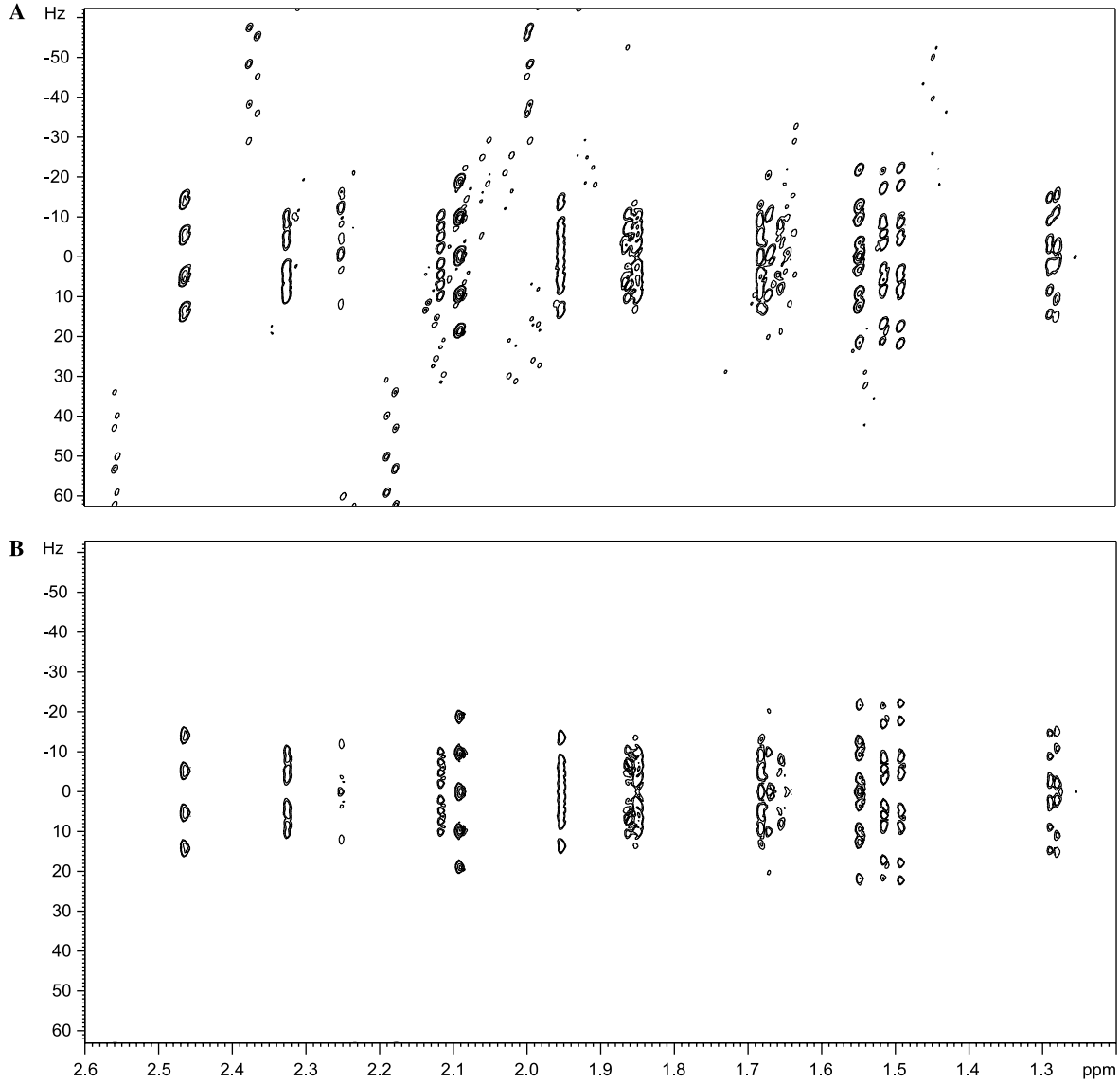

Fig. 8. (A) Tilted DSE *J*-spectrum of dehydroisoandrosterone; the asymmetrically disposed strong coupling artefacts can be removed by symmetrization to give spectrum (B). *Experimental*: the spectrum was acquired at 500 MHz with 8 scans per t_1 increment; spectral widths in the ω_1 and ω_2 dimensions are 125 Hz and 3 kHz, respectively; the acquisition time in t_2 was 2.7 s; 256 t_1 increments were recorded giving a maximum value of 2.0 s; the spectrum has been processed using Gaussian pseudo-echo weighting functions in both dimensions and is displayed in magnitude mode. CTP selection was achieved with pairs of equivalent half-sine shaped 1 ms gradients either side of the two 180° pulses (strength 40 and 60%, respectively).

The DSE *J*-spectrum of 2,3-dibromothiophene is shown in Fig. 5A. When this spectrum is tilted, to give spectrum (B), it is seen that the normal peaks are transformed on to one another by a mirror plane at $\omega_1 = 0$; the strong coupling artefacts do not possess this symmetry property. (Note that this difference in symmetry properties between the normal peaks and the strong coupling artefacts is a consequence of using the double echo sequence; both types of peaks have the same symmetry properties in a *J*-spectrum recorded using the simple sequence, as can be seen in Fig. 2B.)

In the DSE *J*-spectrum the artefacts can therefore be removed using a symmetrization procedure: the intensity at (ω_1, ω_2) is compared with the intensity at $(-\omega_1, \omega_2)$; the higher value is then replaced by the lower value. The symmetrized, tilted DSE *J*-spectrum of 2,3-dibromothiophene and its 45° projection are shown in Figs. 5C and D, respectively; clearly the suppression of the strong coupling artefacts is excellent. The projection is also shown in Fig. 4D, where it can be compared to those obtained by the other methods.

However, the symmetrization procedure is vulnerable to failure in crowded spectra, when two artefacts may appear accidentally at symmetry-related positions. Symmetrization may also cause distortions when the resolutions in the ω_1 and ω_2 dimensions differ significantly.

6. Clean *J*-resolved spectroscopy of dehydroisoandrosterone

The methods described in the previous section generate clean *J*-resolved spectra and "broadband proton decoupled" proton spectra for a two-spin system. To test these experiments on a "real" molecule and on a higher field spectrometer, a sample of dehydroisoan-

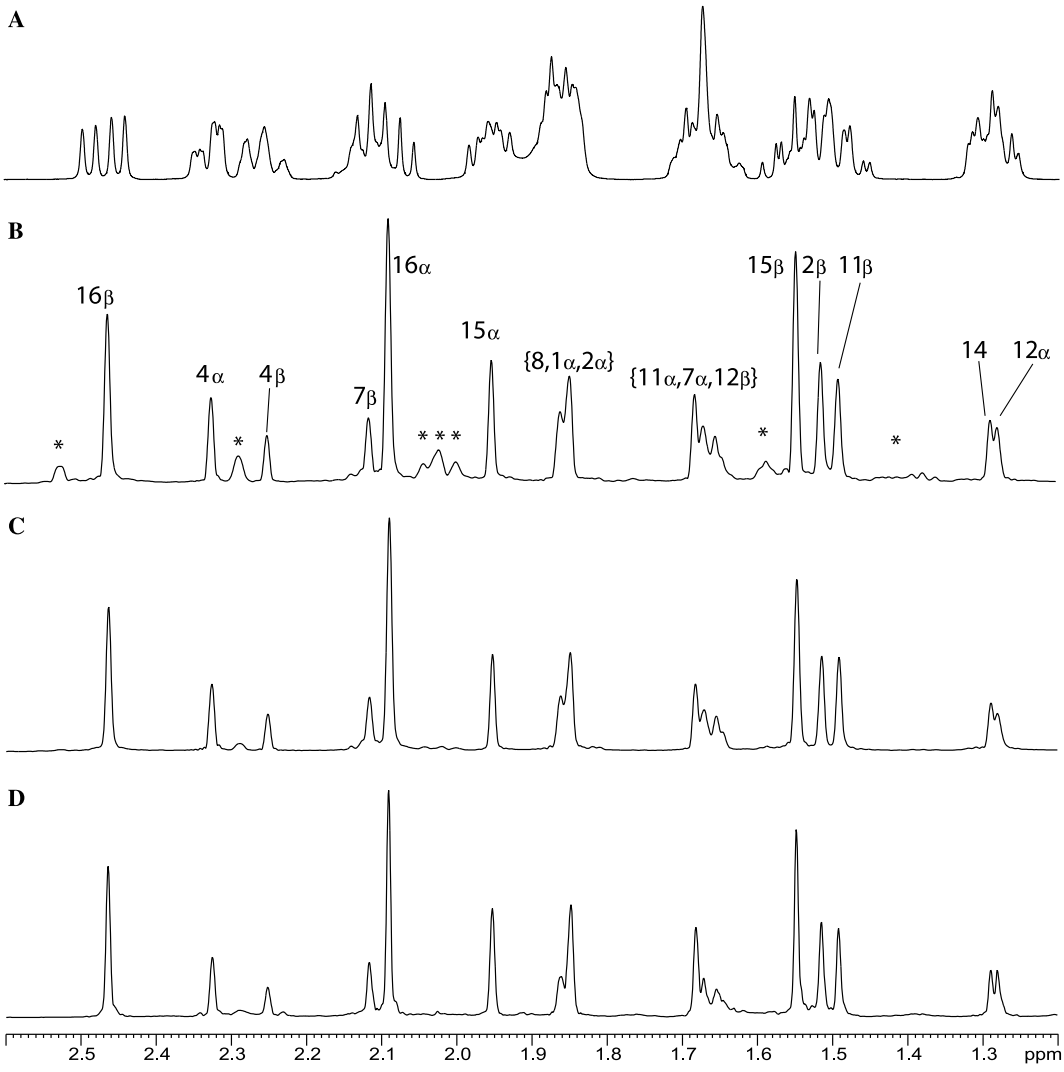

Fig. 9. Projections of the tilted *J*-spectra of dehydroisoandrosterone. Spectrum (A) shows the proton spectrum; spectra (B and C) are projections of the *J*-spectrum and the multiple-scan-filtered *J*-spectrum shown in Figs. 7A and B, respectively. Spectrum (D) is the projection of the symmetrized DSE *J*-spectrum shown in Fig. 8B. Experimental details are given in the captions to Figs. 7 and 8.

drosterone (Fig. 6) was prepared; its proton spectrum at 500 MHz, shown in Fig. 9A, is crowded with overlapping multiplets.

As described in Sections 2 and 3, this crowding is significantly alleviated in the *J*-spectrum, shown in Fig. 7A: chemical shift and coupling information are separated in the two dimensions and many of the multiplets that were overlapping are resolved. However, as described in Section 4, the spectrum contains numerous strong coupling artefacts.

Fig. 7B shows the *J*-spectrum recorded using the multiple-scan filter described in this article. A significant reduction in the intensity of the strong coupling artefacts is evident. The extent of this reduction can be better judged from the projections in Figs. 9B and C. The artefacts have been sufficiently suppressed in Fig. 9C that it can, with caution, be considered as a broadband proton decoupled proton spectrum.

The DSE *J*-spectrum of dehydroisoandrosterone is shown in Fig. 8A and the symmetrized spectrum in Fig. 8B. The projection of the symmetrized spectrum is shown in Fig. 9D. Suppression of the strong coupling artefacts is comparable with that achieved by the multiple-scan filter.

7. Constant-time experiments

Strong coupling artefacts of the type described above for *J*-spectra will appear in any spectrum for which the pulse sequence contains a 180° pulse within the evolution time; a good example is "constant-time" experiments, in which a 180° pulse is moved within a *constant* evolution period. In such experiments, the scalar coupling evolves throughout the constant time, whereas the offset evolves for a time which depends on the position of the 180°. As a result, the evolution in t_1 is unaffected by scalar couplings, so in the ω_1 dimension single peaks appear at the chemical shift instead of multiplets.

In strongly coupled spin systems, the 180° pulse causes coherence transfer, as was described in Section 4. The resulting artefacts can be shown to appear midway between strongly coupled resonances in the ω_1 dimension of the spectrum [4,23].

The multiple-scan and single-scan filters described in Section 5 are applicable to these constant-time experiments. The pulse sequence for constant-time COSY is shown in Fig. 10, together with the multiple-scan- and single-scan-filtered versions. Two-dimensional spectra of 2,3-dibromothiophene recorded using each of these sequences are shown in Fig. 11; cross-sections are also shown.

The strong coupling artefacts are clearly visible in Fig. 11A, both in the two-dimensional spectrum and also in the cross-section. These artefacts are effectively suppressed in Figs. 11B and C.

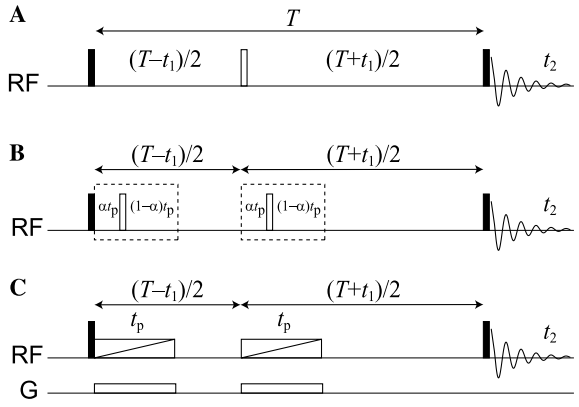

Fig. 10. Constant-time COSY pulse sequences (A) without suppression of strong coupling artefacts, (B) incorporating a multiple-scan filter, and (C) incorporating a single-scan filter.

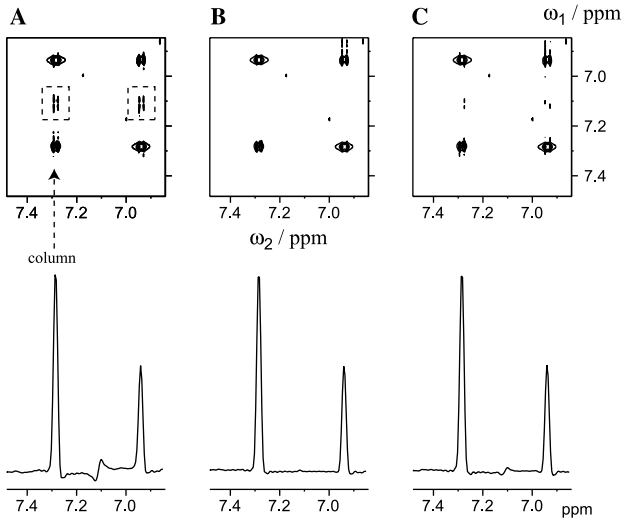

Fig. 11. CT COSY spectra of 2,3-dibromothiophene at 300 MHz (A) without suppression of strong coupling artefacts; (B) using a multiple-scan filter; (C) using a single-scan filter. Cross-sections taken parallel to ω_1 at 7.293 ppm in the ω_2 dimension are shown below each spectrum. *Experimental details*: $T = 385$ ms for each experiment; spectra were acquired with 16 scans per increment, including a two-step phase cycle ($(x, -x)$ on the first pulse and the receiver); the spectral widths in both dimensions are 193 Hz; the acquisition time in t_2 was 2.7 s, and 64 t_1 increments were recorded giving a maximum t_1 of 166 ms; frequency discrimination was achieved by TPPI; spectra were processed using a Gaussian weighting function in the indirect dimension and are phase-sensitive, with both positive and negative contours displayed as solid lines; other relevant details, including the filter parameters, are as for the corresponding *J*-spectroscopy experiments.

8. Conclusion

Scientists prefer to interpret NMR spectra *as if* they are weakly coupled—each multiplet corresponds to a single nuclear environment and each line within the multiplet represents a set of spin states associated with the coupling partners. In practice, the effects of strong cou-

pling are usually evident and these assumptions no longer hold. In a one-dimensional spectrum, the frequencies and intensities of lines are perturbed, though the frequency shifts are usually small and the "roofing" of peak intensities may aid assignment. More insidious are the additional peaks that are generated, particularly in multi-dimensional experiments.

Strong coupling artefacts in *J*-resolved spectra have long been accepted as unavoidable, and most developments of the technique have been directed towards solving the lineshape problem. The methods presented in this article should restore much of the intuitive simplicity of *J*-spectroscopy and other experiments in NMR spectroscopy that incorporate a *J*-resolved or a constant-time dimension.

References

[1] A. Bax, R. Freeman, G.A. Morris, A simple method for suppressing dispersion-mode contributions in NMR spectra: The "pseudo-echo," J. Magn. Reson. 43 (1981) 333–338.

[2] V.A. Mandelshtam, Q.N. Van, A.J. Shaka, Obtaining proton chemical shifts and multiplets from several 1D NMR signals, J. Am. Chem. Soc. 120 (1998) 12161–12162.

[3] G.S. Armstrong, J. Chen, K.E. Cano, A.J. Shaka, V.A. Mandelshtam, Regularized resolvent transform for direct calculation of 45° projections of 2D *J* spectra, J. Magn. Reson. 164 (2003) 136–144.

[4] A. Bax, R. Freeman, Investigation of complex networks of spin–spin coupling by two-dimensional NMR, J. Magn. Reson. 44 (1981) 542–561.

[5] L.N. Ryner, J.A. Sorenson, M.A. Thomas, Localized 2D *J*-resolved ^{1}H MR spectroscopy: Strong coupling effects in vitro and in vivo, Magn. Reson. Imaging 13 (1995) 853–869.

[6] N.M. Loening, NMR studies of molecular diffusion, PhD thesis, Department of Chemistry, University of Cambridge (2000).

[7] L.H. Lucas, W.H. Otto, C.K. Larive, The 2D-*J*-DOSY experiment: Resolving diffusion coefficients in mixtures, J. Magn. Reson. 156 (2002) 138–145.

[8] J.C. Cobas, M. Martín-Pastor, A homodecoupled diffusion experiment for the analysis of complex mixtures by NMR, J. Magn. Reson. 171 (2004) 20–24.

[9] F. Guenneau, P. Mutzenhardt, D. Grandclaude, D. Canet, Measurement of longitudinal and rotating frame relaxation times through fully *J*-decoupled homonuclear spectra, J. Magn. Reson. 140 (1999) 250–258.

[10] G. Bodenhausen, R. Freeman, G.A. Morris, D.L. Turner, NMR spectra of some simple spin systems studied by two-dimensional Fourier transformation of spin echoes, J. Magn. Reson. 31 (1978) 75–95.

[11] A. Kumar, Two-dimensional spin-echo NMR spectroscopy: A general method for calculation of spectra, J. Magn. Reson. 30 (1978) 227–249.

[12] G. Wider, R. Baumann, K. Nagayama, R.R. Ernst, K. Wüthrich, Strong spin–spin coupling in the two-dimensional *J*-resolved 360-MHz ^{1}H NMR spectra of the common amino acids, J. Magn. Reson. 42 (1981) 73–87.

[13] M.J. Thrippleton, New NMR techniques employing spatial variation, PhD thesis, Department of Chemistry, University of Cambridge (2004).

[14] K.F. Riley, M.P. Hobson, S.J. Bence, Mathematical Methods for Physics and Engineering, Cambridge University Press, 1997.

[15] O.W. Sørensen, M. Rance, R.R. Ernst, *z* filters for purging phase- or multiplet-distorted spectra, J. Magn. Reson. 56 (1984) 527–534.

[16] E. McVeigh, A. Yang, E. Zerhouni, Rapid measurement of T1 with spatially selective pre-inversion pulses, Med. Phys. 17 (1990) 131–134.

[17] N.M. Loening, J. Keeler, G.A. Morris, One-dimensional DOSY, J. Magn. Reson. 153 (2001) 103–112.

[18] L. Frydman, T. Scherf, A. Lupulescu, The acquisition of multidimensional NMR spectra within a single scan, Proc. Natl. Acad. Sci. USA 99 (2002) 15858–15862.

[19] M.J. Thrippleton, N.M. Loening, J. Keeler, A fast method for the measurement of diffusion coefficients: One-dimensional DOSY, Magn. Reson. Chem. 41 (2003) 441–447.

[20] N.M. Loening, M.J. Thrippleton, J. Keeler, R.G. Griffin, Single-scan longitudinal relaxation measurements in high-resolution NMR spectroscopy, J. Magn. Reson. 164 (2003) 321–328.

[21] M.J. Thrippleton, J. Keeler, Elimination of zero-quantum interference in two-dimensional NMR spectra, Angew. Chem. Int. Edit. 42 (2003) 3938–3941.

[22] K.E. Cano, M.J. Thrippleton, J. Keeler, A. Shaka, Cascaded *z*-filters for efficient single-scan suppression of zero-quantum coherence, J. Magn. Reson. 167 (2004) 291–297.

[23] Z. Wu, A. Bax, Measurement of homonuclear proton couplings based on cross-peak nulling in CT-COSY, J. Magn. Reson. 151 (2001) 242–252.